ON THE THERMOELECTRIC MAGNETIC FIELD OF SPHERICAL AND CYLINDRICAL INCLUSIONS

submitted for publication to the Journal of Applied Physics

Peter B. Nagy and Adnan H. Nayfeh
Department of Aerospace Engineering and Engineering Mechanics
University of Cincinnati
Cincinnati, Ohio 45221-0070

Introduction

Ordinary thermocouples use the well-known Seebeck effect to measure the temperature at the junction of two different conductors. Ideally, regardless of how high the temperature difference between the hot and cold junctions is, only thermocouples made of different materials, i.e., materials of different thermoelectric powers, will generate thermoelectric signals. This unique feature makes the simple thermoelectric tester one of the most sensitive material discriminators used in nondestructive inspection.[1] However, the inherently imperfect contact between the specimen and the reference electrode can produce a significant thermoelectric signal even if the measuring electrodes are made from the very same material as the specimen.[2] This thermoelectric offset can be reduced, but not entirely eliminated, by decreasing the thermal and electrical resistance between the specimen and the reference electrode (e.g., via cleaning or imposing higher contact pressure). Ultimately, the presence of this imperfect contact limits the detectability of small variations in material properties by the conventional thermoelectric technique. When subtle local variations such as texture, hardening, fatigue damage, or weak impurities are to be detected, the best sensitivity can be achieved by using the surrounding intact material as the reference electrode. This so-called self-referencing method not only provides an ideal reference material, but also automatically eliminates the above mentioned spurious thermoelectric offset caused by having a less than perfect artificial interface between the part to be tested and the surrounding intact reference material.

It was recently demonstrated by Tavrin and Hinken that self-referencing thermoelectric measurements can be also done in an entirely non-contact way by using high-sensitivity SQUID magnetometers to sense the weak thermoelectric currents around inclusions and other types of inhomogeneities when the specimen to be tested is subjected to directional heating or cooling.[3,4] The potential applications of this method cover a very wide range from detection of inclusions, inhomogeneities, and tight cracks to characterization of hardening, fatigue, texture, and residual stresses. However, the primary applications initially will be probably aimed at detection of metallic segregations and other localized inhomogeneities. Therefore the primary goal of this paper was to help lay down the foundations for the development of this new emerging NDE method by modeling the magnetic field produced by thermoelectric currents around spherical and cylindrical inclusions under the influence of external heating or cooling. We investigated how the magnetic signal to be detected depends on (i) the relevant physical properties of the host and the inclusion, (ii) the size of the inclusion, (iii) the depth of the inclusion below the surface of the specimen, (iv) the polarization of the magnetometer, (v) the lift-off distance of the magnetometer from the specimen, and the (vi) direction and (vii) strength of the external heating or cooling applied to the specimen.

To simplify the calculations, all spatial coordinates were normalized to the radius a of the spherical inclusion as $\mathbf{x} = \boldsymbol{x} / a$. The magnetic field can be also written in a normalized form as $\boldsymbol{H} = H_0 \boldsymbol{F}(\mathbf{x})$, where $\boldsymbol{F}(\mathbf{x})$ is a universal spatial distribution

function for all spherical inclusions. The maximum magnitude of the magnetic field is H_0 =a **Ñ***T* s $\boldsymbol{S}_r$ G, where Ñ*T* is the temperature gradient that would prevail in the vicinity of the inclusion if it were not there, s is the electrical conductivity of the host, and S_r is the relative thermoelectric power of the inclusion with respect to the host. Finally, G = 3 / (1 + 2 gs) (2 + 1 / g_k) is the normalized contrast coefficient, where g_s and g_k denote the electrical and thermal conductivity ratios, respectively, between the host and the inclusion. For weak material inhomogeneity (g_s, g_k» 1) the normalized contrast coefficient of a spherical inclusion approaches 1/3.

For a rough estimate of the strength of the magnetic field, let us assume that a modest Ñ*T* = 1 ^oC / cm temperature gradient is maintained in a 7075-T6 aluminum alloy specimen (**s** =1.9 ´10^7 A / Vm) containing a spherical inclusion of *a* = 1 mm. The thermoelectric power of most metals is in the ±10 mV/ ^oC range, therefore we assume that the relative thermoelectric power of the inclusion with respect to the host is a modest S_r= 0.1 mV/ ^oC. With these parameters, we get H_0 » 0.063 A / m or, in terms of magnetic flux density, B_0 » 80 nT. In comparison, the noise limited detection threshold of a SQUID magnetometer is approximately 1 pT over a frequency bandwidth of 1-30 Hz. Most structural metals however have much lower electrical conductivity than aluminum. For example, in Ti-6Al-4V, the most popular aerospace titanium alloy, the electrical conductivity is s» 5.8 ´10^5 . A / Vm, therefore the corresponding magnetic flux density is only B_0» 2.4 nT. Of course, the actual magnetic flux density to be detected further away from the inclusion will be significantly lower than B_0 because of the strong divergency of the field. In the following sections we will calculate the spatial distribution function ***F***(**x**) that describes this divergency effect for different geometrical arrangements.

Half-Space with a Surface-Breaking Spherical Inclusion

Let us assume that the inclusion is cut halfway through by the surface of the specimen as it is shown in Figure 1. In this case, the coupled thermoelectric problem in the remaining half-space is exactly the same as it is in the infinite medium, though the resulting magnetic field is not axisymmetric anymore.

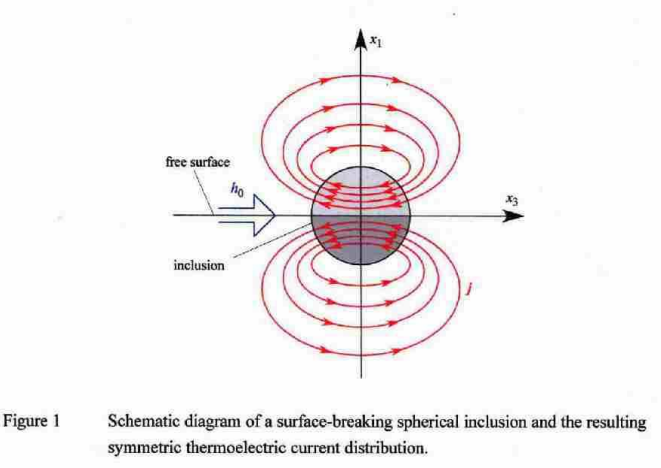

Figure 1 Schematic diagram of a surface-breaking spherical inclusion and the resulting symmetric thermoelectric current distribution.

Figure 1: Schematic diagram of a surface-breaking spherical inclusion and the resulting symmetric thermoelectric current distribution.

Figure 2 shows the surface (x_1 = 0, x_2, x_3) scan of the normal ($\boldsymbol{F}_1$) component of the normalized magnetic field for a surface-breaking spherical inclusion (i.e., a half-sphere with its center lying on the surface). Physically, x_1 represents the normalized vertical lift-off

distance from the surface and x_2 is the normalized horizontal distance from the center of the inclusion in the lateral direction. It is important that the normal component of the magnetic field changes sign as the probe is scanned laterally (i.e., perpendicular to the induced temperature gradient), a characteristic feature that can be exploited for detection purposes. One feature of particular importance from a practical point of view is the so-called lift-off curve, i.e., the dependence of the magnetic field to be detected on the distance between the surface of the specimen and the probe.

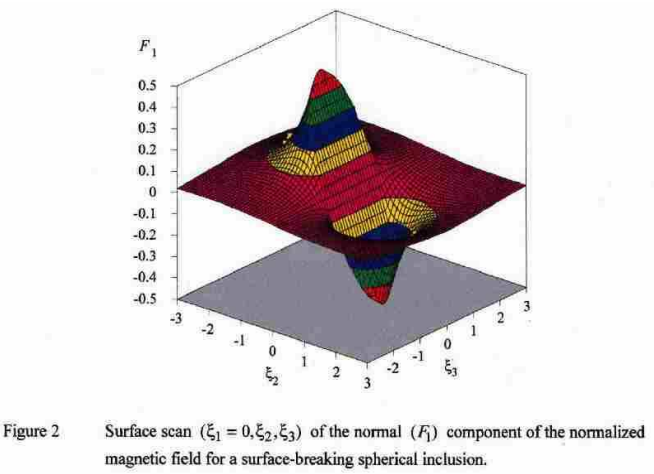

Figure 2 Surface scan $(\xi_1 = 0, \xi_2, \xi_3)$ of the normal (F_1) component of the normalized magnetic field for a surface-breaking spherical inclusion.

Figure 2: Surface scan (x1 = 0, x2, x3) of the normal (*F_1) component of the normalized magnetic field for a surface-breaking spherical inclusion.*

Figure 3 shows the lift-off curves for the maximum normal $\boldsymbol{F}_1$ (x_1, x_2 = - 1,x_3 = 0) and lateral $\boldsymbol{F}_2$ (x_1, x_2 = 0,x_3 = 0) components of the magnetic field above the surface. The normal component, which exhibits a sharp peak at the point of observation, initially decays much faster than the tangential component, although at large distances this difference becomes less pronounced.

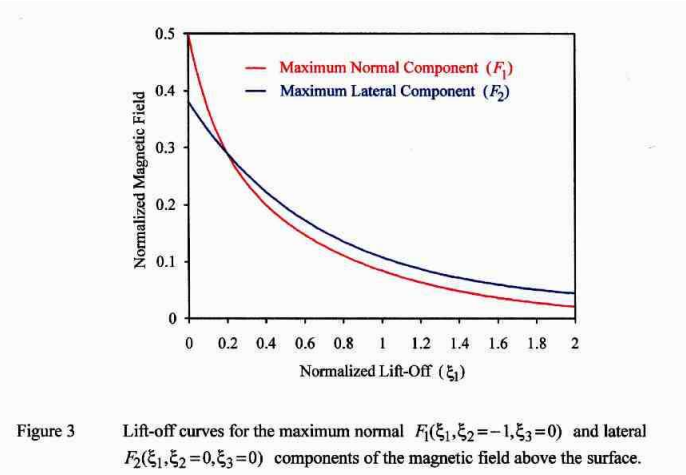

Figure 3 Lift-off curves for the maximum normal $F_1(\xi_1, \xi_2 = -1, \xi_3 = 0)$ and lateral $F_2(\xi_1, \xi_2 = 0, \xi_3 = 0)$ components of the magnetic field above the surface.

Figure 3: Lift-off curves for the maximum normal F_1 (x_1,x_2= -1,x_3=0) and lateral F_2 (x_1,x_2= 0,x_3=0) components of the magnetic field above the surface.

Half-Space with a Subsurface Spherical Inclusion

In order to simulate fully embedded hidden inclusions, we will assume that the center of a spherical inclusion lies below the surface at a depth *d* deeper than its radius, i.e., it is not

breaking the surface at all. In this case, symmetry to the sectioning plane can be retained by considering a pair of spherical inclusions as shown in Figure 4. By assuming that the inclusions are only slightly different from the host or the separation 2*d* between them is large with respect to their radius *a*, the interaction between the two inclusions can be neglected and the resulting thermoelectric current distribution can be approximated simply by superimposing the currents produced by the individual inclusions as calculated for the infinite host.

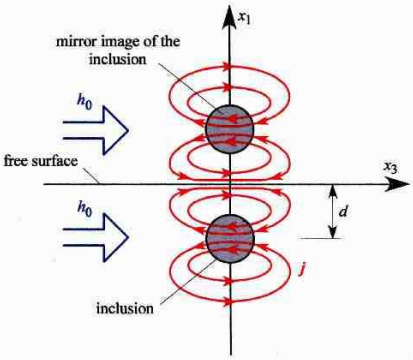

Figure 4 Schematic diagram of the inclusion buried below the surface and its mirror image above it.

Figure 4: Schematic diagram of the inclusion buried below the surface and its mirror image above it.

Figure 5 shows the surface scan (x_1 = 0,x_2, x_3) of the normal (F_1) component of the normalized magnetic field for a subsurface spherical inclusion at a normalized depth d = *d* / *a* = 1. One of the most crucial questions to be answered is how deeply inclusions can be buried and still detected.

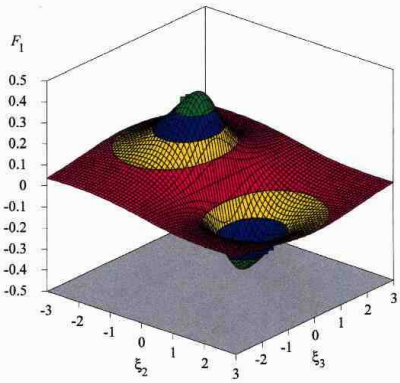

Figure 5 Surface scan $(\xi_1 = 0, \xi_2, \xi_3)$ of the normal (F_1) component of the normalized magnetic field for a subsurface spherical inclusion at a depth $d = a$.

Figure 5: Surface scan (x_1 = 0,x_2,x_3) of the normal F_1 compenent of the normalized magnetic field for a subsurface spherical inclusion at a depth *d* = *a.*

Figure 6 shows the maximum normal and tangential components of the normalized magnetic field on the surface for a subsurface spherical inclusion as a function of the normalized depth d . The magnetic field to be detected decreases proportionally to the square of the depth of the inclusion.

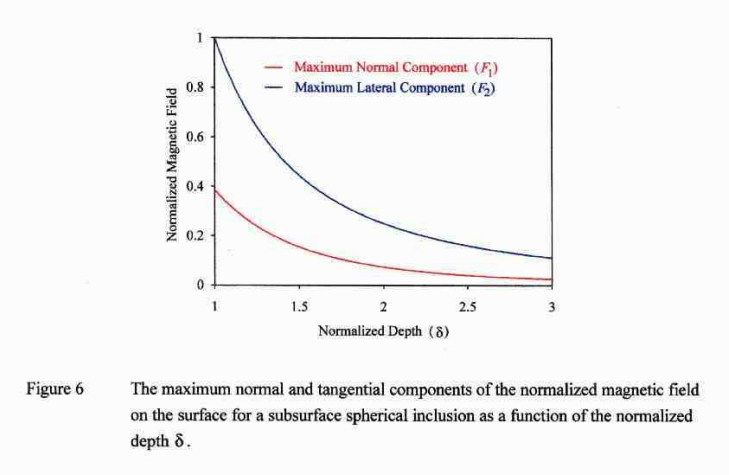

Figure 6 The maximum normal and tangential components of the normalized magnetic field on the surface for a subsurface spherical inclusion as a function of the normalized depth δ.

Figure 6: The maximum normal and tangential components of the normalized magnetic field on the surface for a subsurface spherical inclusion as a function of the normalized depth δ.

References

1 W. Morgner, Mat. Eval. 9, 1081 (1991).
2 J. Hu and P. B. Nagy, Appl. Phys. Lett. 73, 467 (1998).
3 J. H. Hinken and Y. Tavrin, “Thermoelectric SQUID method for the detection of segregations,” in Review of Progress in Quantitative Nondestructive Evaluation, edited by D. O. Thompson and D. E. Chimenti, Vol. 19 (Plenum, New York, to be published).
4 J. H. Hinken and Y. Tavrin, “Detection of segregations in aero engine turbine discs with the thermoelectric SQUID method,” 1999 ASNT Fall Conference (Phoenix, Arizona, October 11-15, 1999).